Alzheimer-mutant γ-secretase complexes stall amyloid β-peptide production

Parnian Arafi[1], Sujan Devkota[1], Masato Maesako[2] and Michael S. Wolfe[1]*

[1]Department of Medicinal Chemistry, University of Kansas, Lawrence, KS, USA

[2]Alzheimer Research Unit, MassGeneral Institute for Neurodegenerative Disease, Massachusetts General Hospital, Harvard Medical School, Boston, MA, USA

Correspondence: mswolfe@ku.edu

Abstract

Missense mutations in the amyloid precursor protein (APP) and presenilin-1 (PSEN1) cause early-onset familial Alzheimer's disease (FAD) and alter proteolytic production of secreted 38-to-43-residue amyloid β-peptides (Aβ) by the PSEN1-containing γ-secretase complex, ostensibly supporting the amyloid hypothesis of pathogenesis. However, proteolysis of APP substrate by γ-secretase is processive, involving initial endoproteolysis to produce long Aβ peptides of 48 or 49 residues followed by carboxypeptidase trimming in mostly tripeptide increments. We recently reported evidence that FAD mutations in APP and PSEN1 cause deficiencies in early steps in processive proteolysis of APP substrate C99 and that this results from stalled γ-secretase enzyme-substrate and/or enzyme-intermediate complexes. These stalled complexes triggered synaptic degeneration in a *C. elegans* model of FAD independently of Aβ production. Here we conducted full quantitative analysis of all proteolytic events on APP substrate by γ-secretase with six additional PSEN1 FAD mutations and found that all six are deficient in multiple processing steps. However, only one of these (F386S) was deficient in certain trimming steps but not in endoproteolysis. Fluorescence lifetime imaging microscopy in intact cells revealed that all six PSEN1 FAD mutations lead to stalled γ-secretase enzyme-substrate/intermediate complexes. The F386S mutation, however, does so only in Aβ-rich regions of the cells, not in C99-rich regions, consistent with the deficiencies of this mutant enzyme only in trimming of Aβ intermediates. These findings provide further evidence that FAD mutations lead stalled and stabilized γ-secretase enzyme-substrate and/or enzyme-intermediate complexes and are consistent with the stalled process rather than the products of γ-secretase proteolysis as the pathogenic trigger.

INTRODUCTION

Alzheimer's disease (AD) poses a significant challenge to global public health as aging populations worldwide face its profound impact on individuals, families, and healthcare systems. The urgent need for accessible and effective disease-modifying therapies underscores the critical importance of unraveling its underlying mechanisms.[1] For over three decades, the amyloid cascade hypothesis has been central in AD research, positing that aggregation of amyloid β-peptides (Aβ), particularly the 42-residue variant (Aβ42), initiates a cascade of events leading to neurodegeneration and dementia.[2] This hypothesis emerged with the discovery of dominant missense mutations in the amyloid precursor protein (APP) associated with early-onset familial Alzheimer's disease (FAD) that alter Aβ production.[3, 4]

The subsequent discovery of FAD mutations in presenilin-1 (PSEN1) and presenilin-2 (PSEN2), catalytic components of γ-secretase complexes responsible for Aβ production from APP C-terminal fragment C99, further reinforced the amyloid hypothesis.[2] These mutations generally increase the ratio of aggregation-prone Aβ42 to more soluble Aβ40. However, the processing of Aβ is complex, involving multiple cleavages of the APP transmembrane domain (TMD) by the membrane-embedded γ-secretase complex, resulting in Aβ peptides through two distinct pathways: C99→Aβ49→Aβ46→Aβ43→Aβ40 and C99→Aβ48→Aβ45→Aβ42→Aβ38 (**Fig. 1A**).[5] Despite these advances, uncertainties persist regarding the assembly states of neurotoxic Aβ species and their roles in AD pathophysiology.[6] Moreover, clinical trials targeting Aβ or its aggregates have shown limited efficacy, prompting a reevaluation of Aβ as the primary driver of the disease process.[7]

The clinical and pathological similarities between early-onset FAD and sporadic late-onset Alzheimer's disease (LOAD) suggest shared underlying disease mechanisms.[8, 9] The monogenic nature of FAD, driven by APP or presenilin mutations, provides a clearer path to elucidating pathogenic mechanisms. FAD mutations in the APP TMD disrupt γ-secretase-mediated proteolysis: Our comprehensive analysis of effects on each proteolytic step for 14 such mutations demonstrated that the first and/or second carboxypeptidase trimming step was

deficient in every case, elevating levels of Aβ peptides of 45 residues and longer.[10] Similarly, we found six PSEN1 FAD-mutant γ-secretase complexes show reduced processive proteolytic function.[11] These PSEN1 mutations were all deficient in the initial endoproteolytic (ε) cleavage of C99 that generates Aβ48 or Aβ49 and the corresponding APP intracellular domain (AICD) co-products, in addition to being deficient in one or more Aβ intermediate trimming steps. Deficient processive proteolysis by FAD mutations was linked to stalled, stabilized γ-secretase enzyme-substrate complexes that triggered age-dependent synaptic degeneration independently of Aβ production in *C. elegans* models of FAD.

In the present study, we have expanded the comprehensive analysis of processive proteolysis of C99 by γ-secretase to include six additional PSEN1 mutations (S169L, S170F, G378E, F386S, A431E, A434T), quantifying each proteolytic step by mass spectrometry as well as interactions between substrate C99 or intermediate Aβs and γ-secretase by fluorescence lifetime imaging microscopy (FLIM). The results demonstrated that all six FAD PSEN1 mutations lead to reduction of multiple proteolytic steps while increasing the stability of enzyme-substrate and/or enzyme-intermediate complexes, findings consistent with our “stalled complex” hypothesis of AD pathogenesis.

RESULTS

FAD-mutant PSEN1 reduces processive proteolysis of C99 by γ-secretase. Six DNA constructs, each encoding an FAD-mutant γ-secretase, were generated, with all PSEN1 mutations corresponding to those under study by the Dominantly Inherited Alzheimer’s Network (DIAN). The selected mutations were S169L, S170F, G378E, F386S, A431E, A434T (**Fig. 1B**). PSEN1 mutations S169L and S170F are in transmembrane domain 3 (TM3), near the hinge region with TMD2. Mutations G378E and F386S are situated in TMD7, close to the catalytic aspartate residue D385 in the conserved GxGD motif. Mutations A431E and A434T are found in a highly conserved region that includes the PALP motif, which is essential for enzymatic activity.[12, 13] The age of onset for these mutations varies as follows: S169L (29-31 years),[14]

S170F (mean 27 years),[15] G378E (38-44 years),[16] F386S (37-58 years),[17] A431E (mean 43 years),[18] and A434T (35 years).[19] Monocistronic pMLINK plasmids encoding human PSEN1, each harboring one of these mutations, were individually prepared via mutagenesis of the wild-type (WT) construct. Each mutant PSEN1 DNA insert was cut out with restriction enzymes from this monocistronic plasmid and inserted into a tricistronic construct encoding the other three components of the γ-secretase complex (nicastrin, Aph-1 and Pen-2) through ligation-independent cloning (LIC). The resulting tetracistronic constructs encode all four components of the protease complex (**Fig. S1**).[20]

The tetracistronic constructs, each encoding either WT or one of the six FAD-mutant forms of the γ-secretase complex, were transiently transfected into human embryonic kidney (HEK) 293F cells, and the expressed protease complexes were subsequently purified.[10, 11] Concurrently, two versions of the recombinant FLAG epitope-tagged version of C99 substrate (C100-Flag) were expressed in *E. coli*: one in normal media, and the other in M9 minimal media containing $^{15}NH_4Cl$ and ^{13}C-glucose as the sole sources of nitrogen and carbon, respectively. Purification provides light and heavy isotope-labeled C100-Flag (**Fig. S2A**). Enzyme purity was verified by Western blot analysis, which demonstrated the presence of all four components of γ-secretase, with PSEN1 autoproteolyzed into N-terminal and C-terminal fragments (NTF and CTF), indicative of maturation of the complex to the catalytically active protease (**Fig. S2B**). Additionally, the quality of the substrates was assessed using matrix-assisted laser desorption/ionization time-of-flight mass spectrometry (MALDI-TOF MS) and silver staining (**Fig. S2C**).

Each purified mutant protease (30 nM) was incubated with saturating levels of the heavy-isotope-labeled substrate (5 μM) at 37 °C for 16 hours. In parallel, the WT enzyme was incubated with light-isotope-labeled C100-Flag substrate. Due to the slow rate for this reaction (WT enzyme k_{cat} = 2 h^{-1}), this long incubation period is still within the linear range for the formation of products (i.e., the enzyme remains saturated with substrate throughout the incubation period).[10] The resulting products for all proteolytic events for each of these samples were then analyzed using various MS

techniques as described below. Due to the hydrophobicity and insolubility of the Aβ products, quantification by direct MS posed significant challenges. Consequently, we focused on analysis of the coproducts (AICDs and small peptides) and indirectly calculating the concentration of the Aβ products.

Rates for the initial endoproteolytic step (ε cleavage) were determined by quantifying AICD species (**Fig. 1A**) using MALDI-TOF MS. We utilized synthetic AICD50-99-Flag and AICD49-99-Flag peptides to construct standard concentration curves by MALDI-TOF MS (**Fig. 1C**). This approach enabled accurate measurements of the production of AICD50-99 (coproduct of Aβ49) and AICD49-99 (coproduct of Aβ48) in both WT and mutant enzyme samples. For all standards and experimental samples, equal concentrations of insulin were added as an internal standard. The standard curves were generated based on the intensity ratio of the AICD parent ion to that of the internal standard (**Fig. 1C**).

Using these standard curves, we calculated concentrations of AICD species in our test samples (**Fig. 1D**). Equal concentrations of both AICD50-99 and AICD49-99 were produced when comparing WT protease incubated with light-isotope C100 to WT protease incubated with heavy-isotope C100. This demonstrates that use of heavy C100 does not affect the concentrations of products formed during the ε cleavage step. Quantification of AICD species was possible for four mutant proteases but not for A431E and A434T, as product concentrations from these two mutant enzymes were below the detection limit (**Fig. 1D**, **S3**), consistent with the known essential role of the PALP motif in proteolytic activity.[12, 13] All FAD-mutant PSEN1-containing enzymes except for F386S exhibited a significant reduction in the production of both AICD50-99 and AICD49-99, which also measures formation of coproducts Aβ49 and Aβ48, respectively. Reduced ε cleavage of APP and Notch substrate has been observed with other PSEN1 FAD mutations.[11, 21, 22] Uniquely, the PSEN1 F386S mutant protease resulted in a significant increase in production of AICD49-99 and similar levels of AICD50-99 compared to those observed with WT protease. Notably, three other mutant enzymes (S169L, G378E, and F386S) likewise biased ε cleavage towards AICD49-99, thereby favoring the Aβ48 → Aβ42 pathway, consistent with previous reports on PSEN1 FAD mutations.[23]

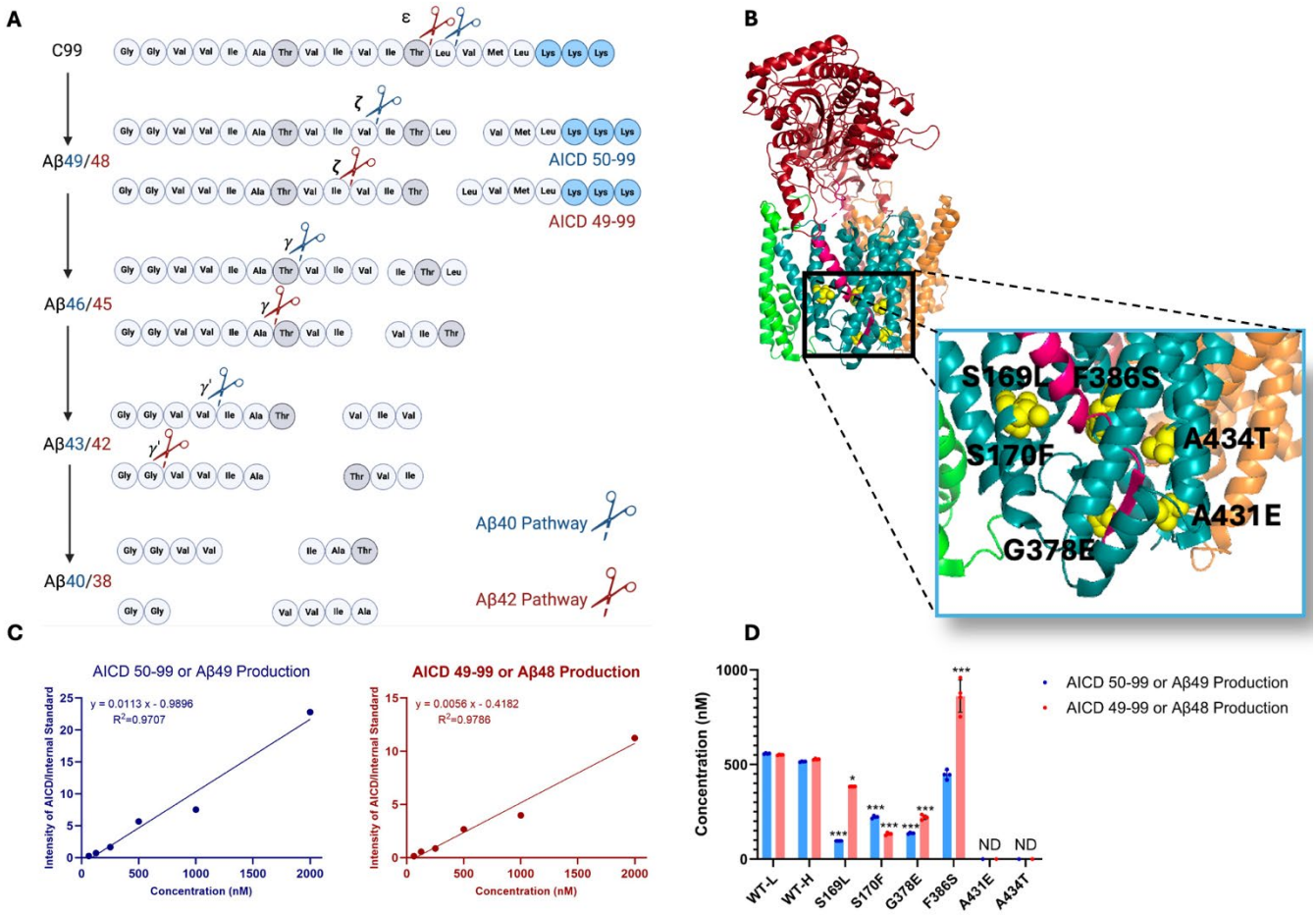

Figure 1. Effects of FAD-mutant PSEN1 on endoproteolysis of C99 by γ-secretase. (A) Diagram of proteolytic cleavage of APP substrate by γ-secretase via two pathways. (B) Ribbon diagram of APP substrate bound to γ-secretase. The six FAD PSEN1 mutations studied in this paper are highlighted in yellow with side chain atoms as spheres. (C) Standard curves for AICD50-99-Flag and AICD49-99-Flag, coproducts of Aβ49 and Aβ48, respectively, were generated by MALDI-TOF using synthetic peptides, with insulin as an internal standard. (D) Quantification of AICD-Flag peptides from enzyme reactions of recombinant APP substrate C100-Flag with WT versus FAD-mutant proteases by MALDI-TOF MS. Standard curves were used to quantify AICD levels for all reactions. Detection limits prevented measurement of AICD-Flag production below 62.5 nM (the lowest standard concentration) for two mutations (A431E and A434T). Consequently, these concentrations are marked as not determined (nd). In all graphs, n = 4. Statistical comparisons between AICD product levels from FAD-mutant versus WT enzymes were performed using unpaired two-tailed t-tests (*$p < 0.05$, **$p < 0.01$, ***$p < 0.001$).

Equal volumes of WT enzyme incubated with light-isotope C100 and PSEN1 FAD-mutant enzymes incubated separately with heavy-isotope C100 were combined in a 1:1 ratio after quenching the reactions (**Fig. 2A**). The 1:1 mixtures were then used to quantify the coproducts of the trimming steps along the two canonical pathways Aβ49→Aβ46→Aβ43→Aβ40 and Aβ48→Aβ45→Aβ42 →Aβ38 via liquid chromatography coupled with tandem MS (LC-MS/MS),[5, 10] as we previously described for six other FAD-mutant enzymes.[11] Mixing of the enzyme reactions after quenching but before analysis allows quantification of each small peptide coproduct formed from WT enzyme and mutant enzyme in the same LC-MS/MS run: Products from WT enzyme incubated with light-isotope C100 have lower mass than products from mutant enzyme incubated with heavy-isotope C100 (**Fig. 2A**). Standard curves were generated for the tri- and tetrapeptide coproducts of each trimming step, using synthetic ITL, VIV, IAT, VIT, TVI, and VVIA peptides, allowing accurate determination of the concentrations of each coproduct generated from all WT and PSEN1 FAD-mutant enzyme reaction mixtures. Equal concentrations of each tri- and tetrapeptide were produced when comparing wild-type (WT) protease incubated with light-isotope C100 to WT protease incubated with heavy-isotope C100, demonstrating that the use of heavy-isotope C100 does not affect the concentrations of products formed during these cleavage steps (**Fig. 2B**).

Quantification of small peptide coproducts from WT vs. PSEN1 FAD-mutant enzyme reactions revealed that each of the six mutations leads to a specific profile of effects on carboxypeptidase trimming. Mutations located within or near the conserved PALP motif,[12, 13] A431E and A434T, exhibited significantly lower levels of trimming coproducts compared to WT and other mutants (**Fig. 2C, S4**). Although AICD levels from A431E and A434T PSEN1 mutant proteases were below those of the lowest standards, very low levels of certain small peptide coproducts were detected within the range of their standard curves. In strong contrast, F386S PSEN1 mutant enzyme produced equal levels of ITL (coproduct of Aβ49→Aβ46) and VIV (coproduct of Aβ46→Aβ43) compared to WT. However, levels of IAT (coproduct of Aβ43→Aβ40) were substantially lower for this mutant enzyme, indicating a buildup of Aβ43 (**Fig. 2C, S4**).

Along the Aβ42 pathway, F386S PSEN1 enzyme produced levels of VIT (coproduct of Aβ48→Aβ45) only slightly lower than WT enzyme; however, because F386S generated increased levels of AICD49-99 (coproduct of C99→Aβ48), this mutant also led to a buildup Aβ48. For mutants S169L, S170F, and G378E, small peptide coproducts were generally lower than those generated from WT (**Fig. 2C, S4**), consistent with their reduced initial ε proteolysis (**Fig. 1D**).

Quantification of all coproducts (AICDs, small peptides) using MS techniques enabled calculation of the percent cleavage for each trimming step in the processive proteolysis of APP by γ-secretase (**Fig. 2D**). That is, given the level of Aβ precursor produced, how much of this precursor was cleaved in the next step? This analysis revealed that none of the mutant enzymes exhibited deficiencies in the Aβ49→Aβ46 or Aβ46→Aβ43 cleavage steps compared to WT enzyme, although percent cleavage could not be determined for A431E and A434T, as these mutant enzymes produced coproducts AICD50-99 and ITL below the limits of detection. The S169L and F386S mutations demonstrated significant changes in the Aβ43→Aβ40 step, with S169L showing a marked increase and F386S showing a decrease compared to WT. All mutations were deficient in the Aβ48→Aβ45 cleavage step, except for S170F, which exhibited an increase in this trimming step. It should be pointed out, however, that this increased percent efficiency of S170F—over 200%--is not possible, suggesting either under-detection of AICD49-99 (production of Aβ48) or over-detection of VIT (degradation of Aβ48) for this mutant enzyme. The reason for this discrepancy is not clear. All mutations except for S169L and A434T were also deficient in the Aβ45→Aβ42 trimming step. Furthermore, all mutations were deficient in the Aβ42 →Aβ38 cleavage process, except for S169L and A431E, which showed increases compared to WT enzyme. We should point out, however, that detected products from A431E and A434T were very low and therefore likely making calculations of percent cleavage unreliable. This detailed analysis highlights specific deficiencies and alterations in the cleavage patterns associated with each mutation, providing a comprehensive and quantitative understanding of how these mutations affect the proteolytic processing of APP by γ-secretase.

Overall, calculation of percent efficiency for each trimming step, along with analysis of effects on initial ε cleavage, revealed that all PSEN1 FAD-mutant proteases are deficient in multiple cleavage steps in processive proteolysis of APP substrate, consistent with previous findings for the other six PSEN1 FAD mutations.[11]

By analyzing the extent of degradation and production of each Aβ peptide, we were able to calculate the levels of each Aβ peptide in the final quenched enzyme reaction mixtures (**Table 1**). We observed a negative value for the concentration of Aβ48 produced from the S170F enzyme, due to the discrepancy pointed out above in quantifying the coproducts of Aβ48 production and degradation. To validate the calculated concentrations of Aβ peptides obtained by LC-MS/MS, we used Aβ40- and Aβ42-specific ELISAs (**Fig. 3A**). The ELISA results were consistent with the calculations from the LC-MS/MS data for all mutations except for F386S. This mutation exhibited higher concentrations of both Aβ40 and Aβ42 when measured by ELISA compared to the calculations derived from MS data (**Fig. 3A vs. 3B**). Because the PSEN1 F386S mutant enzyme produced high levels of Aβ43 (**Table 1**), as previously reported,[24] we tested for cross-reactivity in the ELISAs with synthetic Aβ43 peptide. We found that the putatively Aβ40- and Aβ42-specific ELISAs both cross-reacted with Aβ43 (**Table S1**), which can explain the observed discrepancies with F386S enzyme. According to the ELISA results, all six PSEN1 FAD-mutant enzymes produced lower levels of Aβ40 and Aβ42 compared to WT, consistent with our previous findings with six other PSEN1 FAD mutations.[11] Mutants S169L, G378E, and F386S showed an increased Aβ42/Aβ40 ratio by both ELISA and LC-MS/MS (**Fig. 3**). In contrast, Aβ42/Aβ40 produced from the S170F mutant enzyme was equivalent to that of WT by both methods. Mutants A431E and A434T appear to increase Aβ42/Aβ40 by LC-MS/MS; however, these two FAD-mutant enzymes produce such low levels of peptide coproducts that the calculated ratio is not reliable. By ELISA, only Aβ42 was detectable from A431E and A434T mutant enzymes, precluding calculation of Aβ42/Aβ40 ratios.

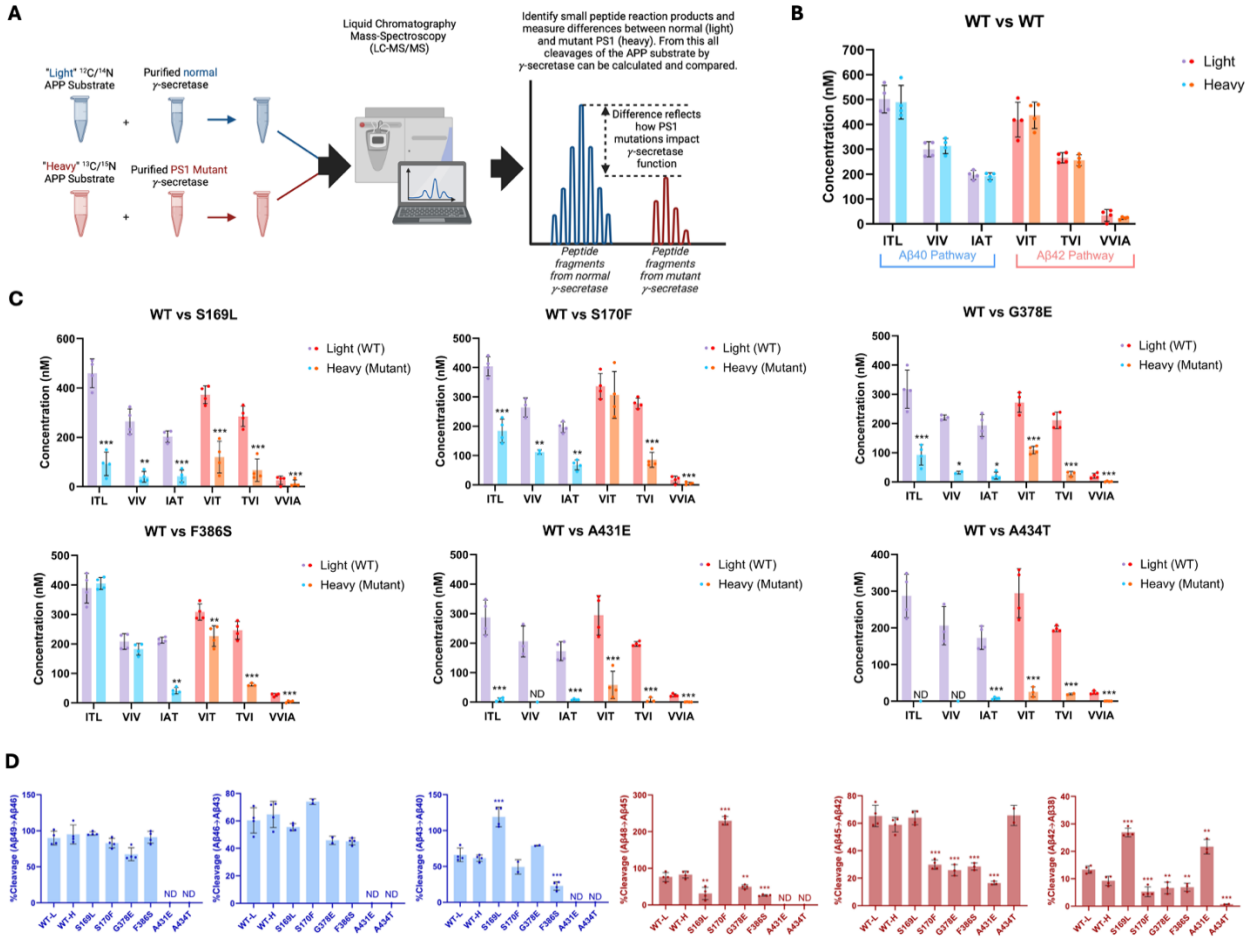

Figure 2. Alzheimer-mutant PSEN-1 affects the processive proteolysis of C99 by γ-secretase. (A) Schematic representation of the reaction mixtures and their preparation, analyzed by LC-MS/MS for the detection of tri- and tetrapeptide coproducts. (B) Comparison of tri- and tetrapeptide coproduct concentrations between WT enzyme incubated with light-isotope substrate and WT enzyme incubated with heavy-isotope substrate, as analyzed by LC-MS/MS. (C) Bar graphs illustrating all coproduct formation for specific mutations. For the Aβ49→Aβ40 pathway, blue and purple bars represent the first, second, and third trimming steps. Red and orange bars denote trimming steps for the Aβ48→Aβ38 pathway. Purple and red bars indicate coproducts formed by WT γ-secretase, while blue and orange bars indicated coproducts formed by FAD-mutant enzyme. (D) Bar graphs showing the percentage cleavage efficiency for each trimming step for mutant enzyme compared to WT enzyme. Cleavage events where the precursor Aβ peptide level was zero (i.e., no detected coproduct) are marked as not determined (nd). For each graph, n = 4 and statistical significance was determined using unpaired two-tailed t-tests comparing FAD-mutant with WT enzyme reactions (*$p < 0.05$, **$p < 0.01$, ***$p < 0.001$).

Table 1. Calculated concentration (nM) of each Aβ variant resulting from processing APP substrate by WT vs. FAD-mutant γ-secretase.[a]

PSEN-1	Aβ49	Aβ46	Aβ43	Aβ40	Aβ48	Aβ45	Aβ42	Aβ38
WT-L	56.0	201.7	103.3	196.9	131.5	153.3	231.6	34.2
WT-H	26.3	176.3	121.0	191.8	91.2	180.9	232.0	23.7
S169L	3.7	52.7	-2.8	42.5	264.6	52.8	53.8	12.9
S170F	38.4	128.3	-2.8	67.9	-173.5	221.2	80.8	4.9
G378E	44.2	76.7	-5.5	21.6	112.2	88.9	19.2	1.3
F386S	41.4	222.9	140.9	41.2	634.8	180.1	43.3	4.3
A431E	ND	8.3	-8.8	8.8	ND	52.6	5.1	0.4
A434T	ND	0	-7.9	7.9	ND	9.2	9.4	0.3

[a] Calculated Aβ species produced from reaction mixtures containing 5 μM C100Flag incubated at 37 °C for 16 h with 30 nM of either WT or FAD-mutant γ-secretase complexes. Calculations were based on concentrations of coproducts, where [Aβx] = [coproduct of Aβx production] – [coproduct of Aβx degradation] (e.g., [Aβ48] = [AICD49-99] - [VIT]).

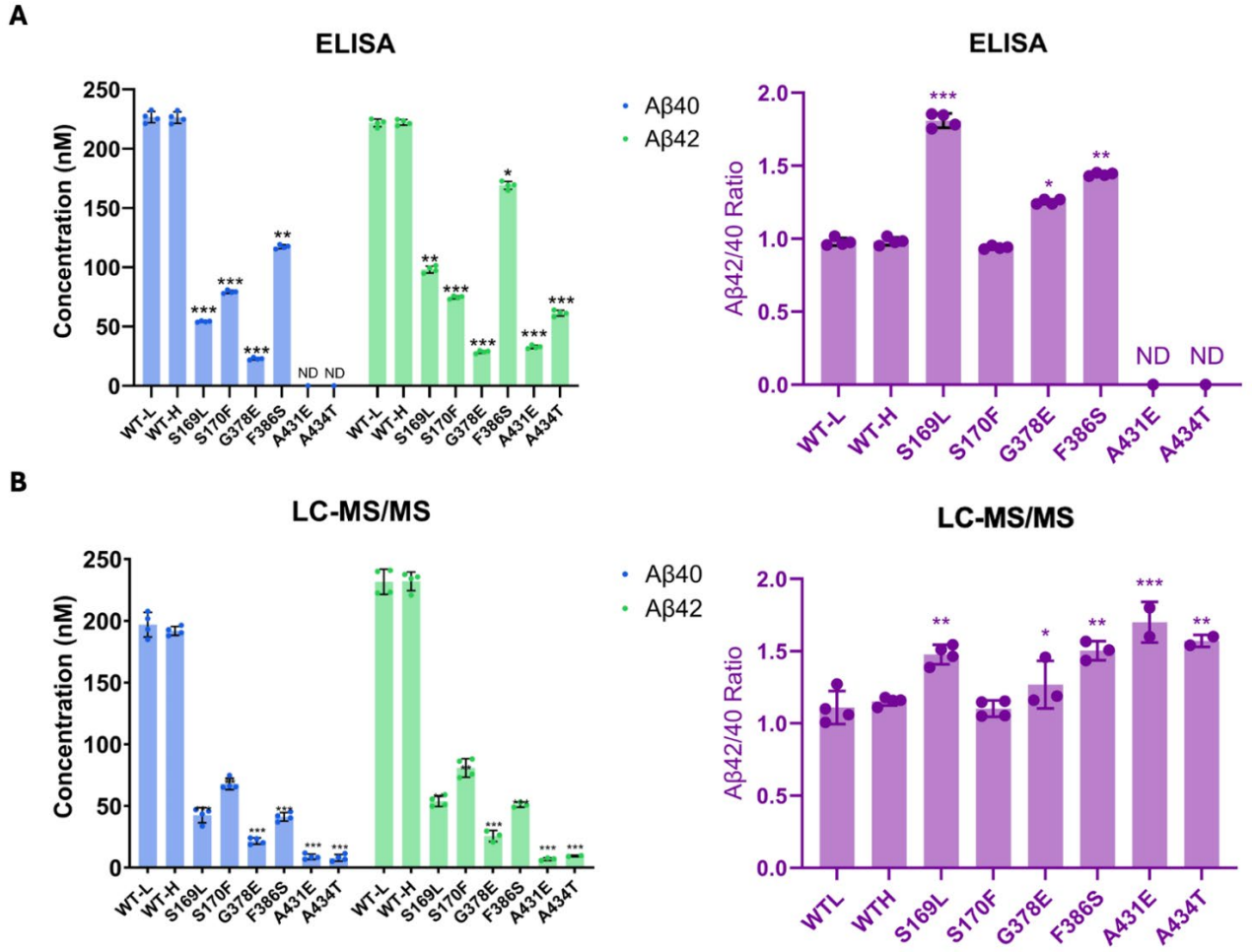

Figure 3. Comparison of Aβ40 and Aβ42 concentrations determined by LC-MS/MS vs. ELISA. Final Aβ40 and Aβ42 concentrations upon incubation of purified γ-secretase with C100Flag and the resulting Aβ42/Aβ40 ratios assessed by (A) ELISAs and (B) LC-MS/MS calculations. N=4 with unpaired two-tailed T-tests comparing FAD-mutant to WT enzyme reactions (*p≤ 0.05, **p≤ 0.01, ***p≤ 0.001).

PSEN1 FAD mutations stabilize γ-secretase enzyme-substrate complexes. To test effects of FAD mutations on the stability of γ-secretase enzyme-substrate (E-S) complexes, we conducted fluorescence lifetime imaging microscopy (FLIM) in intact cells.[25] WT or FAD-mutant PSEN1 was co-expressed with C99 substrate in HEK293 cells in which endogenous PSEN1 and PSEN2 were knocked out through CRISPR/Cas9 gene editing.[26] C99 substrate construct consisted of human APP C99 flanked by N-terminal signal peptide and C-terminal near-infrared fluorescence protein: miRFP720 (C99-720) (**Fig. 4A**). Transfected cells were fixed and permeabilized and treated with primary antibodies that bind to the N-terminal region of C99/Aβ (mouse antibody 6E10) and with an epitope on the nicastrin component of γ-secretase (rabbit antibody NBP2-57365) that lies in close proximity to the N-terminal region of bound C99/Aβ. Secondary antibodies conjugated to fluorophore (anti-mouse IgG antibody conjugated with Alexa Fluor 488 and anti-rabbit IgG antibody conjugated with Cy3) were then added. In this experimental design, reduction in the fluorescence lifetime of the Alexa Fluor 488, through fluorescence resonance energy transfer to Cy3, indicates E-S complex detection. Importantly, use of rabbit antibody toward a distal region in the γ-secretase complex results in no change in Alexa Fluor 488 fluorescence lifetime.[11]

For each but one PSEN1 FAD mutant tested, Alexa Fluor 488 fluorescence lifetime is reduced compared to that of WT PSEN1 (**Fig. 4B,C**), consistent with increased stability of E-S complexes. The miRFP720 fusion to the C-terminus of C99 provides a means of distinguishing between C99-rich regions in the cells (low ratio of 6E10 to C99-720) from Aβ-rich regions (high ratio of 6E10 to C99-720) (**Fig. 4A**).[11, 27, 28] Although the PSEN1 F386S mutant did not show an overall fluorescence lifetime reduction compared to WT, when differentiating C99-rich regions versus Aβ-rich regions (**Fig. 4D**), fluorescence lifetime was significantly reduced in Aβ-rich regions and not C99-rich regions (**Fig. 4E vs. 4F**). This finding is completely consistent with the results of proteolytic analysis, as PSEN1 F386S is the only mutant that was not deficient in ε cleavage but was deficient in specific trimming steps, especially Aβ43→Aβ40 and Aβ48→Aβ45.

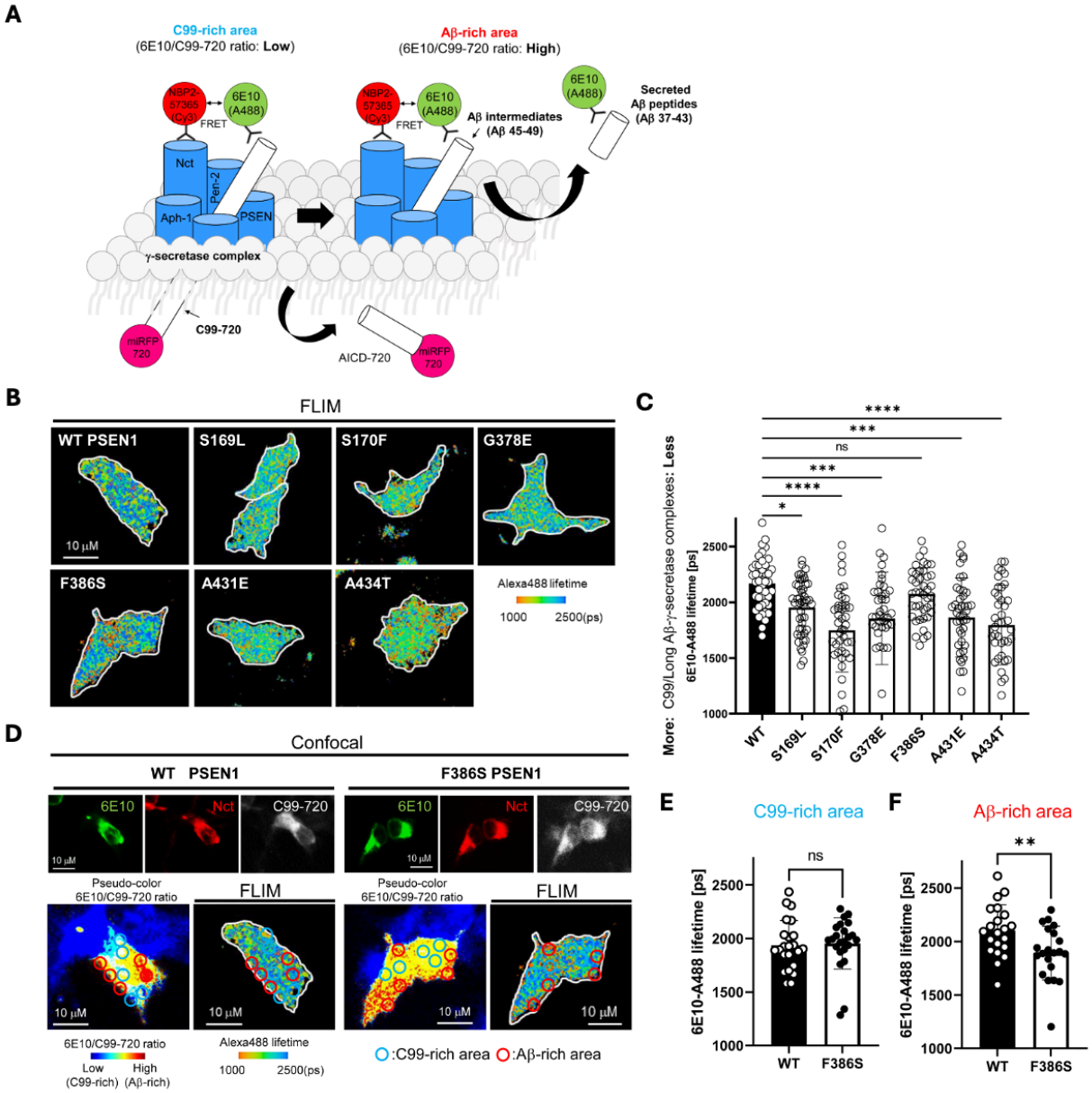

Figure 4. FAD-mutant PS1 stabilizes γ-secretase E-S interaction. (A) Design of fluorescence lifetime imaging microscopy (FLIM) set-up to detect E-S complexes of γ-secretase and C99/Aβ-intermediates. 6E10-Alexa Fluor™ 488 over C99-720 fluorescence ratio (6E10-A488/C99-720 ratio) enables distinguishing C99-rich and Aβ-rich subcellular compartments. (B) PSEN1/2 dKO HEK293 cells were co-transfected with C99-720 and WT or FAD mutant PSEN1. Transfected cells were immunostained with anti-C99/Aβ (mouse 6E10) and anti-nicastrin (rabbit NBP2-57365) primary antibodies and Alexa Fluor™ 488 (FRET donor) or Cy3 (acceptor)-conjugated anti-mouse and anti-rabbit IgG secondary antibodies, respectively. The donor 6E10-Alexa Fluor™ 488 (6E10-A488) lifetime was measured by FLIM. Energy transfer from the donor to the acceptor results in shortening of the donor lifetime. Scale bars, 10 μm. (C) 6E10-A488 lifetimes

were analyzed in randomly selected ROIs (N=40-47 from 6-8 cells), highlighting increased E-S complexes in the cells with FAD PSEN1 mutants, except F386S, compared to WT controls. One-way ANOVA and Tukey's multiple comparisons test; n.s., $p > 0.05$; *$p < 0.05$; **$p < 0.01$; ***$p < 0.001$; ****$p < 0.0001$. (D) Representative images of confocal, pseudo-color analysis to identify C99 or Aβ-rich subcellular areas and corresponding FLIM in wild-type or F386S PSEN1 expressing cells. Scale bars, 10 μm. (E) In the areas with lower 6E10-A488/C99-720 ratios (i.e., C99-rich areas), 6E10-A488 lifetimes were not different between the cells with WT PSEN1 and those with F386S mutant. N=21 ROIs. (F) On the other hand, 6E10-A488 lifetimes were significantly shorter in the cells expressing F386S mutant PSEN1 compared to wild-type controls in Aβ-rich ROIs (N=23). Unpaired T-test **$p < 0.01$.

DISCUSSION

The persistent challenge of developing effective therapeutics for Alzheimer's disease (AD) continues to spark contentious debates within the biomedical research community on the identity of the pathogenic trigger. The "amyloid cascade hypothesis," long a central focus in AD research, has faced significant scrutiny, particularly due to its failure to consistently correlate brain amyloid plaque burden with cognitive decline.[29] Difficulties in pinpointing disease drivers of AD and in discovering effective therapeutics suggest that entities and processes beyond Aβ might play pivotal roles in initiating neurodegeneration. Focusing on FAD could simplify identification of pathogenic mechanisms, as these rare variants of AD are caused by dominant missense mutations in the substrate and enzyme that produce Aβ. This targeted approach may provide clearer insights into the molecular underpinnings of AD and facilitate the development of more effective treatments.

In this study, we focused on six FAD PSEN1 mutations that are among those under investigation by the Dominantly Inherited Alzheimer Network (DIAN),[30-32] conducting a comprehensive and quantitative analysis of processive proteolysis of APP substrate C99 by γ-secretase. Our analysis revealed that five of the six mutations exhibited substantial deficiencies in the initial cleavage event (ε cleavage), consistent with our previously reported findings for six other FAD PSEN1 mutations.[11] The exception was the F386S mutation, which was deficient in

several trimming steps (Aβ43→Aβ40, Aβ48→Aβ45, Aβ45→Aβ42, and Aβ42→Aβ38) but not in ε cleavage. This was surprising, because this mutation is immediately adjacent to one of the two catalytic aspartate residues (D385) and was therefore expected to decrease ε cleavage.

To further explore the impact of these mutations, we employed fluorescence lifetime imaging microscopy (FLIM). Stabilization of FAD-mutant E-S complexes while stalled in their proteolytic activities was supported by reduced fluorescence lifetimes of labeled antibody probe combinations targeting the E-S complexes. Based on our FLIM studies, all six FAD PSEN1 mutations tested showed stabilized E-S complexes. Five of these mutations, stabilized overall γ-secretase E-S interactions, while the F386S mutant stabilized only γ-secretase/Aβ and not γ-secretase/C99 interactions. Together, FLIM data and comprehensive analysis of all cleavage steps involved in the processive proteolysis of APP substrate by γ-secretase revealed that each of these mutations is deficient in multiple cleavage events due to stalled and stabilized E-S complexes (**Fig. 5**).

The FAD S169L mutant was shown to be the second least deficient in ε cleavage among the six in ε cleavage, as demonstrated by quantification of AICDs using MALDI-TOF. Similarly, FLIM studies indicate that this mutation results in the smallest decrease in overall fluorescence lifetime after F386S, suggesting a small but still significant increase in stabilization of overall E-S complexes. According to recent reports by Guo *et al.*, and Odorčić *et al.* of cryoelectron microscopy (cryoEM) structures of γ-secretase bound to C99 and Aβ intermediates, S169 is a key residue involved in processive proteolysis. These two groups suggested that FAD mutants destabilize E-S complexes, specifically mentioning the loss of an H-bonding interaction with S169 mutants as the rationale.[33, 34] However, static structures such as those captured by cryoEM cannot account for dynamic changes in protein conformation, such as the decreased E-S complex flexibility we observed for FAD mutations by molecular dynamics simulations.[11]

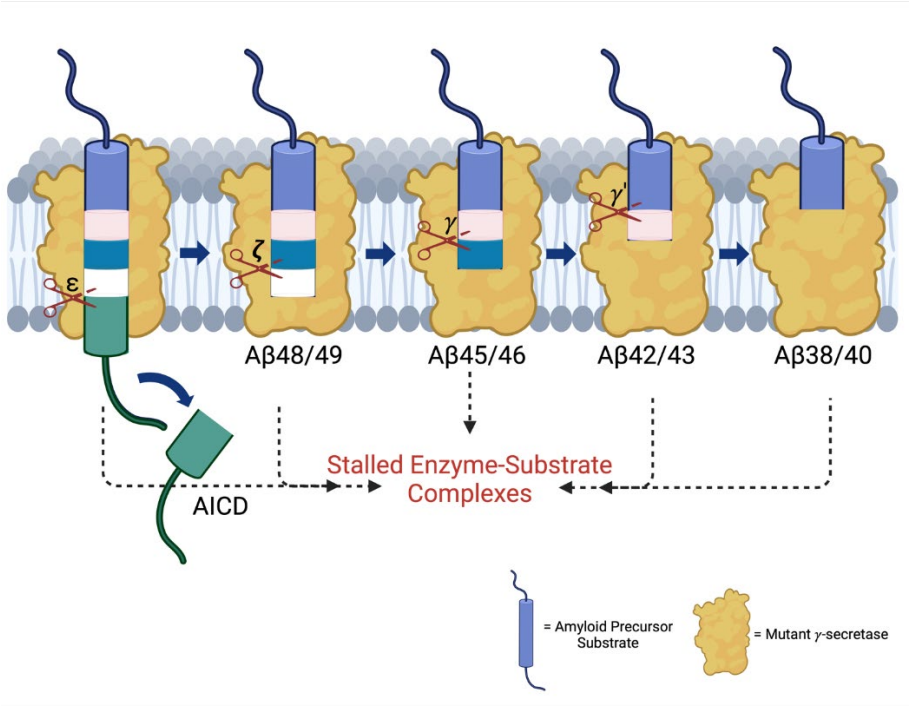

Figure 5. FAD mutations lead to stalled processive proteolysis of APP substrate by γ-secretase. PSEN1 FAD-mutant γ-secretase complexes are deficient in specific cleavage steps. Enzyme-substrate/intermediate complexes are stalled at these stages.

The PSEN1 A431E and A434T FAD-mutant enzymes exhibited the most pronounced deficiencies in all cleavage events compared to WT. These mutations are located within or near the highly conserved PALP motif, which plays a critical role in the active site conformation and catalytic activity of γ-secretase.[12, 13] This motif is essential for the recognition of APP substrate by γ-secretase.[35] The C-terminal PALP motif and the rest of PSEN1 TMD9 are also integral to the formation of the catalytic pore of the protease.[36] Consequently, the observed deficiencies in A431E and A434T can be attributed to the disruption of these crucial structural and functional elements. Nevertheless, our FLIM results suggest these FAD-mutant proteases can still interact with C99 and form stable E-S complexes. In this context, it should be noted that no FAD-mutant enzyme is completely deficient in proteolytic activity; substrate interaction with the mutant protease is apparently critical to pathogenesis. Consistent with this idea, true loss of function of γ-secretase—due to dominant mutations in PSEN1 and other components of the protease

complex that lead to nonsense-mediated decay (i.e., haploinsufficiency)—cause a hereditary skin disease, not neurodegeneration.[37]

While an elevated Aβ42/Aβ40 ratio is commonly cited as a hallmark of FAD mutations, our results show that S170F did not lead to an increase in this ratio. This finding is consistent with a previous study, which analyzed Aβ40 and Aβ42 production from 138 FAD PSEN1 mutations using purified γ-secretase and APP substrate, which revealed that many FAD mutations do not elevate Aβ42/Aβ40.[38] Among those mutations that do increase the ratio, the effect is primarily due to a reduction in Aβ40 production, with some mutations resulting in minimal production of both Aβ variants.

The findings reported herein are consistent with our working hypothesis that FAD mutations lead to stalled γ-secretase E-S complexes that contribute to pathogenesis (**Fig. 5**). These stalled complexes—observed in FAD regardless of the specific deficient cleavage steps of the mutation—can trigger synaptic loss *in vivo*, even in the absence of Aβ production.[11] The "stalled complex hypothesis" posits that stabilized E-S complexes, even in the absence of Aβ42 or any other proteolytic product, can initiate pathogenesis. In this context, γ-secretase activators (GSAs) that rescue stalled E-S complexes offer a promising therapeutic strategy by potentially rescuing deficient proteolytic function and thereby reducing levels of stalled E-S complexes, without over-activating cleavage of other substrates (which are limited by prior rate-determining ectodomain shedding).[39] Such activators would be distinct from γ-secretase modulators (GSMs), which selectively reduce Aβ42 levels by stimulating Aβ42→Aβ38. This approach may complement therapies targeting tau aggregation, lipid metabolism, and other Alzheimer-associated pathways, potentially synergizing with emerging drug candidates.[40]

LIMITATIONS OF THE STUDY

While detailed and quantitative studies of the impact of FAD mutations on all proteolytic stages of γ-secretase processing of C99 have been carried out here, these experiments utilized purified enzymes and substrates in a detergent-solubilized system. This system differs

significantly from the cell membrane environment, which is characterized by complex lipid and protein compositions and dynamic microdomains that can affect protein folding, stability, and function. Therefore, the effects of these mutations on γ-secretase processing of C99 may vary considerably when studied in detergent-solubilized systems compared to their natural membrane environment. However, we previously noted that detergent-solubilized and reconstituted proteoliposome systems give similar ratios of AICD49-99/AICD50-99 and Aβ42/Aβ40.[10] While using MALDI-TOF instead of western blotting provided more accurate quantification of AICDs, we encountered challenges with lower concentrations of AICDs produced by mutations such as A431E and A434T. The concentrations of AICDs in these mostly deficient mutations fell below the detection limit of our instrument, limiting our ability to assess their levels accurately. In addition, FLIM studies relied on overexpression of PSEN1 and C99-720, which could lead to artifacts.

ACKNOWLEDGMENTS

We thank L. Liu (Harvard Medical School/Brigham and Women's Hospital) for HEK293 cells with PSEN1/2 doubly knocked out through genome editing. This work was supported by U.S. National Institutes of Health (NIH) grants AG66986 (to M.S.W.) and AG079569 (to J. Chhatwal; Co-PI M.S.W.). P. Arafi was supported by an undergraduate research award from NIH grant P20 GM103418.

MATERIALS AND METHODS

Key Resources Table

Reagent or Resources	Source	Identifier
Antibodies		
Mouse anti-Flag M2	Sigma-Aldrich	Cat. No. F1804; RRID Ab_262044
Mouse anti-FLAG M2-agarose beads	Sigma-Aldrich	Cat. No. A2220; RRID:AB_10063035
Mouse anti-PSEN1-NTF	Bio-Legend	Cat. No. 823401; RRID:AB_2564868
Rabbit anti-nicastrin	Novus Biologicals	Cat. No. NBP2-57365
Presenilin 1 (D39D1) Rabbit mAb-CTF	Cell Signalling	Cat. No. 5643
Rabbit anti-Aph-1a, 245-265 (C terminus) Antibody	Bio-Legend	Cat. No. 823101
Goat anti-Mouse IgG (H+L) Secondary Antibody, HRP	Invitrogen	Cat. No. 62-6520
Anti-rabbit IgG, HRP-linked Antibody	Cell Signalling	Cat. No. 7074
Precision Plus Protein™ WesternC™ Blotting Standards	Bio-Rad	Cat. No. 1610376
Precision Protein StrepTactin-HRP Conjugate	Bio-Rad	Cat. No. 1610381
Mouse anti-Ab 6E10	Bio-Legend	Cat. No. 803001; RRID:AB_2564653
Rabbit anti-nicastrin	Novus Biologicals	Cat. No. NBP2-57365
Alexa FluorTM 488-conjugated goat anti-mouse IgG	ThermoFisher	Cat. No. A32723; RRID:AB_2633275
Cy3-conjugated goat anti-rabbit IgG	ThermoFisher	Cat. No. A10520; RRID:AB_2534029
Bacterial and virus strains		
NEB 5-alpha Competent E. coli (DH5α)	New England Biolabs	Cat. No. C2987H
E. coli BL21 DE3	New England Biolabs	Cat. No. C2530H
Chemicals, peptides, and recombinant proteins		
Expi293™ Expression Medium	ThermoFisher Scientific	Cat. No. A1435101
13C glucose	Cambridge Isotope Laboratories	Cat. No. CLM-1396
15NH4Cl	Cambridge Isotope Laboratories	Cat. No. NLM-467
PacI restriction enzyme	New England Biolabs	Cat. No. R0547S
SwaI restriction enzyme	New England Biolabs	Cat. No. R0604S
T4 DNA Polymerase	New England Biolabs	Cat. No. M0203L
DOPC (1,2-dioleoyl-sn-glycerol-3-phosphocholine)	Avanti Polar Lipids	Cat. No. 850375
DOPE (1,2-dioleoyl-sn-glycero-3-phosphoethanolamine)	Avanti Polar Lipids	Cat. No. 850725
Digitonin	Goldbio	Cat. No. D-180-5
Peptides VIT, ITL, VIV, TVI, IAT and VVIAA	New England Peptide	Custom synthesized
beta-Amyloid Peptide (1-43) (Aß43)	Abcam	Cat. No. 134500-80-4
AICD 50-99	Chemical Biology Synthetic Core at The University of Kansas	N/A
AICD 49-99	Chemical Biology Synthetic Core at The University of Kansas	N/A
ProteoMass™ Insulin MALDI-MS	Sigma-Aldrich	Cat. No. 11070-73-8
Opti-MEM™ I Reduced Serum Medium	Gibco	Cat. No. 31985062
SuperSignal™ West Femto Maximum Sensitivity Substrate	ThermoFisher Scientific	Cat. No. 34094
ExpiFectamine™ 293 Transfection Kit	Gibco	Cat. No. A14524
LB Broth	Fisher Scientific	Cat. No. BP1426-2
UltraPure™ Ethidium Bromide	Invitrogen	Cat. No. 15585011
MES SDS Running Buffer	Invitrogen	Cat. No. B0002
Western Blot Stripping Buffer	ThermoFisher Scientific	Cat. No. 21059
NuPAGE™ Transfer Buffer	Invitrogen	Cat. No.NP00061
TAE Buffer, Molecular Biology Grade (Tris-acetate-EDTA)	Promega	Cat. No. V4271
SimplyBlue™ SafeStain	Invitrogen	Cat. No. LC6060
NuPAGE™ Bis-Tris Mini Protein Gels, 10%, 1.0–1.5 mm	Invitrogen	Cat. No. NP0315BOX
NuPAGE™ LDS Sample Buffer (4X)	Invitrogen	Cat. No. NP0007
NuPAGE™ Sample Reducing Agent (10X)	Invitrogen	Cat. No. NP0009
EDTA (0.5 M), pH 8.0	ThermoFisher Scientific	Cat. No. R1021
TriTrack DNA Loading Dye (6X)	ThermoFisher Scientific	Cat. No. R1161
Penicillin-Streptomycin	Gibco	Cat. No. 15140122
Critical commercial assays		
QuikChange Lightning Multi-Site Directed Mutagenesis kit	Agilent	Cat. No. 210513
Amyloid b-peptide 1-40 ELISA kit	Invitrogen	Cat. No. KHB3481
Amyloid b-peptide 1-42 ELISA kit	Invitrogen	Cat. No. KHB3441

Pierce™ BCA Protein Assay Kits	ThermoFisher Scientific	Cat. No. 23225
PureLink™ HiPure Plasmid Filter Maxiprep Kit	Invitrogen	Cat. No. K210017
QIAwave Plasmid Miniprep Kit	Qiagen	Cat. No. 27204
QIAquick Gel Extraction Kit	Qiagen	Cat. No. 28704
Experimental models: Cell lines		
Expi293F™ Cells	ThermoFisher Scientific	Cat. No. A14527
HEK293 cells with PSEN1/2 double knockout by CRISPR	Lei Liu, Brigham and Women's Hospital	Liu et al. (ref. 26)
Oligonucleotides		
DNA primer for S169L PSEN1 mutagenesis: catgcctggcttattatattatctctattgttgctgttc	Invitrogen	Custom synthesized
DNA primer for S170F PSEN1 mutagenesis: catgcctggcttattatatcatttctattgttgctgttc	Invitrogen	Custom synthesized
DNA primer for G378E PSEN1 mutagenesis: gacccagaggaaagggaagtaaaacttggattg	Invitrogen	Custom synthesized
DNA primer for F386S PSEN1 mutagenesis: cttggattgggagattccattttctacagtgttctg	Invitrogen	Custom synthesized
DNA primer for A431E PSEN1 mutagenesis: gccattttcaagaaagaattgccagctcttccaatc	Invitrogen	Custom synthesized
DNA primer for A434T PSEN1 mutagenesis: aagaaagcattgccaactcttccaatctccatc	Invitrogen	Custom synthesized
Recombinant DNA		
pMLINK-PSEN1	Y. Shi (Westlake University, China)	Lu et al., Ref. 20
pMLINK-Aph1 (with C-terminal HA epitope tag)	Y. Shi (Westlake University, China)	Lu et al., Ref. 20
pMLINK-NCT (with C-terminal V5 and 6XHIS epitope tags)	Y. Shi (Westlake University, China)	Lu et al., Ref. 20
pMLINK-Pen-2 (with N-terminal STREP and FLAG epitope tags)	Y. Shi (Westlake University, China)	Lu et al., Ref. 20
pMLINK-PSEN1-Aph1-NCT-Pen-2	This study	N/A
pMLINK-PSEN1(S169L)-Aph1-NCT-Pen-2	This study	N/A
pMLINK-PSEN1(S170F)-Aph1-NCT-Pen-2	This study	N/A
pMLINK-PSEN1(G378E)-Aph1-NCT-Pen-2	This study	N/A
pMLINK-PSEN1(F386S)-Aph1-NCT-Pen-2	This study	N/A
pMLINK-PSEN1(A431E)-Aph1-NCT-Pen-2	This study	N/A
pMLINK-PSEN1(A434T)-Aph1-NCT-Pen-2	This study	N/A
pET22b-C100-FLAG	In-house	Li et al., Ref. 41
pcDNA3.1-C99 miRFP720	Co-author M. Maesako	Devkota et al., Ref. 11
Software and algorithms		
Prism 9 version 9.5.1	GraphPad	https://www.graphpad.com
Fiji ImageJ 1.53c	NIH	https://imagej.nih.gov/
AzureSpot	Azure Biosystems	https://azurebiosystems.com/
MassLynx	Waters	https://www.waters.com
SPC-830 (fluorescence lifetime imaging microscopy data collection)	Becker & Hickl GmbH	https://www.becker-hickl.com
SPC Image software version 2.5 (fluorescence lifetime imaging microscopy analysis	Becker & Hickl GmbH	https://www.becker-hickl.com
MATLAB (pseudo-color fluorescence lifetime imaging microscopy)	MathWorks	https://www.mathworks.com

Cell lines

Expi293F™ Cells, a human embryonic kidney (HEK) cell line purchased from Invitrogen, were utilized to produce γ-secretase complexes protein. HEK293 cells with PSEN1/2 double knockout by CRISPR (ref. 26), a gift of Dr. Lei Liu (Brigham and Women's Hospital, Harvard Medical School, Boston, MA), were used for transfection and fluorescence lifetime imaging microscopy.

Cell culture conditions

Expi293F™ cells were cultured in Expi293™ expression medium (ThermoFisher Scientific, A1435101). Transient transfection occurred once the cell density reached 3 x 10^6 cells/mL. The cells were kept at

37 °C, shaken at 125 rpm, and under 8% CO_2. Harvesting took place when cell viability decreased to 75%.

Bacterial strain and culture

E. coli DH5α was employed for molecular cloning and plasmid preparation and was cultured in LB medium at 37°C with constant shaking. *E. coli* BL21 (DE3) was used for the transduction and expression of the γ-secretase substrate C100Flag,[41] grown in LB medium at 37 °C with continuous shaking until OD_{600} reached 0.8, at which point expression was induced using 0.5 mM IPTG.

Methods

Wild-type and FAD-mutant γ-secretase constructs

Direct attempts to mutate the PSEN-1 within the vector, according to Sun et al.,[38] were unsuccessful due to the large size of the pMLINK tetra-cistronic vector used in this experiment. This plasmid contains genetic codes for all four components of γ-secretase: Nicastrin (NCT), Presenilin Enhancer 2 (Pen2), Anterior Pharynx-defective 1 (Aph1), and Presenilin-1 (PSEN1). To overcome this challenge, we developed a step-by-step ligation-independent cloning (LIC) method in *E. coli*, combined with restriction digestion of both the insert and vector, which allowed for the successful insertion of mutations. Four monocistronic pMLINK vectors were generated following established methods: pMLINK-PSEN1, pMLINK-Aph1 (bearing a C-terminal HA epitope tag), pMLINK-NCT (with C-terminal V5 and 6XHIS epitope tags), and pMLINK-Pen-2 (featuring N-terminal STREP and FLAG epitope tags).[20] Each vector contains LINK1 and LINK2 sequences flanking the gene of interest. LINK1 includes a PacI restriction site, while LINK2 contains both PacI and SwaI restriction sites. To create a tricistronic plasmid containing genetic codes for NCT, Pen2, and Aph1, we employed a two-step process. First, we used LIC in *E. coli* to combine NCT and Pen2 through restriction digestion, forming a bicistronic plasmid. The pMLINK-Pen-2 and pMLINK-NCT vectors were treated with restriction enzymes PacI and SwaI, respectively. Both fragments were then electrophoresed through a 1% agarose gel to separate and purify the Pen2 DNA and to linearize and isolate the NCT vector. The Pen2 fragment and the linearized pMLINK-NCT vector were treated with T4 polymerase for 20 minutes at ambient temperature in the presence of dCTP or dGTP, respectively. The purified T4 polymerase-treated Pen2 fragment was inserted into the purified linearized pMLINK-NCT by LIC to create a bicistronic pMLINK-NCT-Pen-2 vector. Subsequently, we further modified the bicistronic plasmid by including Aph1 through another round of restriction digestion and LIC in *E. coli*, resulting in a tricistronic plasmid. Finally, to create a mutated tetra-cistronic plasmid, we performed Multi multi-site-directed mutagenesis on the PSEN1 and inserted this monocistronic construct into the tricistronic plasmid through additional rounds of restriction digestion and LIC in *E. coli*. (See Fig. S1 for illustration)

γ-Secretase expression and purification

γ-Secretase was produced and purified from Expi293F™ cells as described in earlier studies.[42-44] Briefly, Expi293F™ cells were grown in Expi293™ expression medium supplemented with penicillin-streptomycin until they reached a density of 3 x 10^6 cells/mL. Before transfection, the medium was exchanged for fresh Expi293™ expression medium (without penicillin-streptomycin). For the transfection process, 100 µg of the pMLINK tetracistronic vector and 320 µL of ExpiFectamine™ 293 Reagent were mixed in 12 mL of Opti-MEM™ I Reduced Serum Medium and incubated at room temperature for 20 minutes. The resulting ExpiFectamine™ 293/plasmid DNA complexes were then added to the cell culture. After 20 hours, ExpiFectamine™ 293 Transfection Enhancer 1 and Enhancer 2 were added, and the cells were cultured until their viability dropped to 75%. The cells were then harvested by centrifugation at 300 x g for 5 minutes and resuspended in a buffer containing 50 mM MES (pH 6.0), 150 mM NaCl, 5 mM $CaCl_2$, and 5 mM $MgCl_2$. They were lysed by passing twice through a French press. Unbroken cells and debris were removed by centrifugation at 3000 x g for 10 minutes, and the supernatant was ultracentrifuged at 100,000 x g for 1 hour to obtain the membrane pellet. The membrane pellet was washed with 0.1 M sodium bicarbonate (pH 11.3) by sequentially passing through syringes with 18-, 22-, 25-, and 27-gauge needles, followed by another ultracentrifugation at 100,000 x g for 1 hour. The pellet was resuspended in 50 mM HEPES (pH 7), 150 mM NaCl, and 1% CHAPSO, and incubated at 4 ºC with shaking for 1 hour. This mixture was ultracentrifuged again at 100,000 x g. The supernatant was incubated with anti-FLAG M2-agarose beads in TBS containing 0.1% digitonin for 16 hours at 4 ℃ with shaking. The beads were washed three times with TBS/0.1% digitonin before eluting the γ-secretase complex using a buffer with 0.2 mg/mL FLAG peptide in TBS/0.1% digitonin. The eluate was stored at -80 ℃ until needed.

C100-FLAG expression and purification

Two versions of C100-Flag, light and heavy isotope-labeled C100-Flag were prepared. *E. coli* BL21 cells transformed with C100-FLAG construct in pET22b vector[41] were grown in media at 37 ℃ with 180 rpm shaking until OD_{600} reached 0.8. The standard media and M9 minimal media with 20% ^{13}C-glucose (Cambridge Isotope Laboratories) and $^{15}NH_4Cl$ (Cambridge Isotope Laboratories) were used to produce light isotope labeling and heavy isotope-labeled C100-Flag substrate respectively. M9 Minimal media composition: 3.4 g of anhydrous N_2HPO_4, 8.794g of KH_2PO_4, 0.25 g of NaCl, 0.5 g of $^{15}NH_4Cl$, 10 mL of 20% ^{13}C glucose, 1 mL of 1 M $MgSO_4$-$7H_2O$, 10 µL of 1 M $CaCl_2$-$2H_2O$, 500 µL of 0.5% thiamine-HCl, 5 mL of BME vitamin solution (Sigma-Aldrich), and 10 µL of 1 M $FeSO_4$ -$7H_2O$ were dissolved into 500 mL sterilized and deionized water. Cells were induced with 0.5 mM IPTG and cultured for 3 hours. After harvesting by centrifugation, the cells were resuspended in lysis buffer (25 mM Tris, pH 8, and 1% Triton X-100) and lysed by passing through a French press three times. The cleared lysate was incubated with anti-FLAG M2-agarose beads (Sigma-Aldrich) at 4 °C for 16 hours

with shaking. The beads were washed three times with lysis buffer, and the C100-FLAG protein was eluted using a buffer containing 100 mM glycine at pH 2.7 and 0.25% NP-40, followed by neutralization with Tris buffer at pH 8 and stored at -80 °C. The composition and integrity of C100-FLAG were confirmed by SDS-PAGE with western blotting and MALDI-TOF mass spectrometry.

Antibodies and western blot analysis for γ-secretase expressed from Expi293F™ cells and C100 expressed from *E. Coli* cells

The following antibodies were used: Anti-Nicastrin (Novus Biologicals, NBP2-57365), Anti-PSEN-1-NTF (Bio-Legend, 823401), anti-PSEN-1-CTF (Cell Signaling, 5643), Anti-Aph-1 (Bio-Legend, 823101), and Anti-Flag M2 (Sigma-Aldrich, F1804). Western blot analysis was carried out using standard procedures. Protein levels of the purified γ-secretase enzyme and the C100 substrate were quantified using a BCA assay (Thermo Fisher Scientific, USA) and normalized for different expression levels based on band intensity. These proteins were separated by SDS-PAGE and transferred onto PVDF membranes. Immunoblotting was then performed and visualized using the enhanced chemiluminescence method.

***In vitro* γ-secretase assay**

The *in vitro* γ-secretase assay was conducted as previously detailed [12]. In summary, 30 nM of either wild-type or FAD mutant γ-secretase was preincubated for 30 minutes at 37 ℃ in an assay buffer containing 750 μL of 50 mM HEPES (pH 7.0), 150 mM NaCl, 125 μL of DOPC (1,2-dioleoyl-sn-glycero-3-phosphocholine), and 125 μL of DOPE (1,2-dioleoyl-sn-glycero-3-phosphoethanolamine). The reactions were initiated by adding the light- or heavy-isotope form of the C100-FLAG substrate to a final concentration of 5 mM and incubated at 37℃ for 16 hours. The reactions were terminated by flash freezing in liquid nitrogen and stored at -20 ℃.

Tri- and tetrapeptide quantification by LC-MS/MS

As previously mentioned, small peptides were examined by LC-MS/MS utilizing an ESI Quadrupole Time-of-Flight (Q-TOF) mass spectrometer (Q-TOF Premier, Waters) [12]. Before being injected into a C18 analytical chromatography column, the reaction mixtures containing light C100-FLAG/WT γ-secretase and heavy C100-Flag/FAD γ-secretase were mixed 1:1. The reaction mixtures were then eluted using a step gradient of 0.08% aqueous formic acid, acetonitrile, isopropanol, and a 1:1 acetone/dioxane mixture. Tandem MS was used to determine which three collision-induced dissociation fragments were the most prevalent for each small peptide. A C18 analytical chromatography column was loaded with different amounts of the synthetic peptide standards (>98% purity, New England Peptide) after they had been dissolved in an assay buffer for LC-MS/MS analysis. Employing an ion

mass width of 0.02 unit, the signals from the three most abundant ions were added to produce a peptide chromatographic area. The "V" mode was used for data acquisition.

Quantification of AICD Species by Mass Spectrometry

AICD-FLAG in the reaction mixture was immunoprecipitated with anti-FLAG M2 beads (Sigma-Aldrich) in 10mM MES pH 6.5, 10 mM NaCl, 0.05% DDM detergent for 16 hours at 4 ℃. AICD products were eluted from the anti-FLAG beads with acetonitrile: water (1:1) with 0.1% trifluoroacetic acid. In parallel, different concentrations of AICD standards (2500 nM, 2000 nM, 1000 nM, 500 nM, 250 nM, 125 nM, and 62.5 nM) were prepared using synthetic peptides. To all samples and standards, 5 nM of ProteoMass™ Insulin MALDI-MS was added as an internal standard. Finally, the elutes were analyzed on a Bruker Autoflex MALDI-TOF mass spectrometer.

Quantification of Aβ40 and Aβ42 by ELISA

To quantify Aβ peptides, we analyzed reactions from *in vitro* cleavage assays involving purified γ-secretase complexes and the C100-FLAG substrate using specific ELISA kits from Invitrogen, in accordance with the manufacturer's instructions.

Fluorescence lifetime imaging microscopy (FLIM)

Fluorescence emissions were collected using the ET525/50m-2p filter (Chroma Technology Corp, Bellows Falls, VT). The donor Alexa Fluor™ 488 lifetime was recorded using a high-speed photomultiplier tube (MCP R3809; Hamamatsu photonics, Hamamatsu City, Japan) and a time-correlated single-photon counting acquisition board (SPC-830; Becker & Hickl GmbH, Berlin, Germany). The acquired FLIM data were analyzed using SPC Image software (Becker & Hickl GmbH). Pseudo-colored images corresponding to the ratios of 6E10-Alexa Fluor™ 488 over C99-720 emission were generated in MATLAB (MathWorks, Natick, MA).

REFERENCES

[1] Li, X., Feng, X., Sun, X., Hou, N., Han, F., and Liu, Y. (2022) Global, Regional, and National Burden of Alzheimer's Disease and Other Dementias, *Front Aging Neurosci 14*, https://doi.org/10.3389/fnagi.2022.937486.

[2] Selkoe, D. J., and Hardy, J. (2016) The amyloid hypothesis of Alzheimer's disease at 25 years, *EMBO Mol Med 8*, 595-608.

[3] Hardy, J., and Allsop, D. (1991) Amyloid deposition as the central event in the aetiology of Alzheimer's disease, *Trends Pharmacol Sci 12*, 383-388.

[4] Selkoe, D. J. (1991) The molecular pathology of Alzheimer's disease, *Neuron 6*, 487-498.

[5] Takami, M., Nagashima, Y., Sano, Y., Ishihara, S., Morishima-Kawashima, M., Funamoto, S., and Ihara, Y. (2009) γ-Secretase: successive tripeptide and tetrapeptide release from the transmembrane domain of β-carboxyl terminal fragment, *J Neurosci 29*, 13042-13052.

[6] Benilova, I., Karran, E., and De Strooper, B. (2012) The toxic Aβ oligomer and Alzheimer's disease: an emperor in need of clothes, *Nat Neurosci 15*, 349-357.

[7] Kepp, K. P., Robakis, N. K., Høilund-Carlsen, P. F., Sensi, S. L., and Vissel, B. (2023) The amyloid cascade hypothesis: an updated critical review, *Brain 146,* 3969-3990

[8] Bateman, R. J., Aisen, P. S., De Strooper, B., Fox, N. C., Lemere, C. A., Ringman, J. M., Salloway, S., Sperling, R. A., Windisch, M., and Xiong, C. (2011) Autosomal-dominant Alzheimer's disease: a review and proposal for the prevention of Alzheimer's disease, *Alzheimer Res Therap 3*, 1.

[9] Morris, J. C., Weiner, M., Xiong, C., Beckett, L., Coble, D., Saito, N., Aisen, P. S., Allegri, R., Benzinger, T. L. S., Berman, S. B., Cairns, N. J., Carrillo, M. C., Chui, H. C., Chhatwal, J. P., Cruchaga, C., Fagan, A. M., Farlow, M., Fox, N. C., Ghetti, B., Goate, A. M., Gordon, B. A., Graff-Radford, N., Day, G. S., Hassenstab, J., Ikeuchi, T., Jack, C. R., Jagust, W. J., Jucker, M., Levin, J., Massoumzadeh, P., Masters, C. L., Martins, R., McDade, E., Mori, H., Noble, J. M., Petersen, R. C., Ringman, J. M., Salloway, S., Saykin, A. J., Schofield, P. R., Shaw, L. M., Toga, A. W., Trojanowski, J. Q., Vöglein, J., Weninger, S., Bateman, R. J., and Buckles, V. D. (2022) Autosomal dominant and sporadic late onset Alzheimer's disease share a common in vivo pathophysiology, *Brain 145*, 3594-3607.

[10] Devkota, S., Williams, T. D., and Wolfe, M. S. (2021) Familial Alzheimer's disease mutations in amyloid protein precursor alter proteolysis by γ-secretase to increase amyloid β-peptides of >45 residues, *J Biol Chem. 296:100281*.

[11] Devkota, S., Zhou, R., Nagarajan, V., Maesako, M., Do, H., Noorani, A., Overmeyer, C., Bhattarai, S., Douglas, J. T., Saraf, A., Miao, Y., Ackley, B. D., Shi, Y., and Wolfe, M. S. (2024) Familial Alzheimer mutations stabilize synaptotoxic γ-secretase-substrate complexes, *Cell Rep 43*, 113761.

[12] Wang, J., Brunkan, A. L., Hecimovic, S., Walker, E., and Goate, A. (2004) Conserved "PAL" sequence in presenilins is essential for γ-secretase activity, but not required for formation or stabilization of γ-secretase complexes, *Neurobiol Dis 15*, 654-666.

[13] Tomita, T., Watabiki, T., Takikawa, R., Morohashi, Y., Takasugi, N., Kopan, R., De Strooper, B., and Iwatsubo, T. (2001) The first proline of PALP motif at the C terminus of presenilins is obligatory for stabilization, complex formation, and γ-secretase activities of presenilins, *J Biol Chem 276*, 33273-33281.

[14] Taddei, K., Kwok, J. B., Kril, J. J., Halliday, G. M., Creasey, H., Hallupp, M., Fisher, C., Brooks, W. S., Chung, C., Andrews, C., Masters, C. L., Schofield, P. R., and Martins, R. N. (1998) Two novel presenilin-1 mutations (Ser169Leu and Pro436Gln) associated with very early onset Alzheimer's disease, *Neuroreport 9*, 3335-3339.

[15] Snider, B. J., Norton, J., Coats, M. A., Chakraverty, S., Hou, C. E., Jervis, R., Lendon, C. L., Goate, A. M., McKeel, D. W., Jr., and Morris, J. C. (2005) Novel presenilin 1 mutation (S170F) causing Alzheimer disease with Lewy bodies in the third decade of life, *Arch Neurol 62*, 1821-1830.

[16] Lanoiselée, H. M., Nicolas, G., Wallon, D., Rovelet-Lecrux, A., Lacour, M., Rousseau, S., Richard, A. C., Pasquier, F., Rollin-Sillaire, A., Martinaud, O., Quillard-Muraine, M., de la Sayette, V., Boutoleau-Bretonniere, C., Etcharry-Bouyx, F., Chauviré, V., Sarazin, M., le Ber, I., Epelbaum, S., Jonveaux, T., Rouaud, O., Ceccaldi, M., Félician, O., Godefroy, O., Formaglio, M., Croisile, B., Auriacombe, S., Chamard, L., Vincent, J. L., Sauvée, M., Marelli-Tosi, C., Gabelle, A., Ozsancak, C., Pariente, J., Paquet, C., Hannequin, D., and Campion, D. (2017) APP, PSEN1, and PSEN2 mutations in early-onset Alzheimer disease: A genetic screening study of familial and sporadic cases, *PLoS Med 14*, e1002270.

[17] Raux, G., Guyant-Maréchal, L., Martin, C., Bou, J., Penet, C., Brice, A., Hannequin, D., Frebourg, T., and Campion, D. (2005) Molecular diagnosis of autosomal dominant early onset Alzheimer's disease: an update, *J Med Genet 42*, 793-795.

[18] Dumois-Petersen, S., Gallegos-Arreola, M. P., Magaña-Torres, M. T., Perea-Díaz, F. J., Ringman, J. M., and Figuera, L. E. (2020) Autosomal dominant early onset Alzheimer's disease in the Mexican state of Jalisco: High frequency of the mutation PSEN1 c.1292C>A and phenotypic profile of patients, *Am J Med Genet C Semin Med Genet 184*, 1023-1029.

[19] Jiao, B., Tang, B., Liu, X., Xu, J., Wang, Y., Zhou, L., Zhang, F., Yan, X., Zhou, Y., and Shen, L. (2014) Mutational analysis in early-onset familial Alzheimer's disease in Mainland China, *Neurobiol Aging 35*, 1957.e1951-1956.

[20] Lu, P., Bai, X. C., Ma, D., Xie, T., Yan, C., Sun, L., Yang, G., Zhao, Y., Zhou, R., Scheres, S. H., and Shi, Y. (2014) Three-dimensional structure of human γ-secretase, *Nature 512*, 166-170.

[21] Song, W., Nadeau, P., Yuan, M., Yang, X., Shen, J., and Yankner, B. A. (1999) Proteolytic release and nuclear translocation of Notch-1 are induced by presenilin-1 and impaired by pathogenic presenilin-1 mutations, *Proc Natl Acad Sci USA 96*, 6959-6963.

[22] Bentahir, M., Nyabi, O., Verhamme, J., Tolia, A., Horre, K., Wiltfang, J., Esselmann, H., and De Strooper, B. (2006) Presenilin clinical mutations can affect γ-secretase activity by different mechanisms, *J Neurochem 96*, 732-742.

[23] Sato, T., Dohmae, N., Qi, Y., Kakuda, N., Misonou, H., Mitsumori, R., Maruyama, H., Koo, E. H., Haass, C., Takio, K., Morishima-Kawashima, M., Ishiura, S., and Ihara, Y. (2003) Potential link between amyloid β-protein 42 and C-terminal fragment γ49-99 of β-amyloid precursor protein, *J Biol Chem 278*, 24294-24301.

[24] Liu, L., Lauro, B. M., He, A., Lee, H., Bhattarai, S., Wolfe, M. S., Bennett, D. A., Karch, C. M., Young-Pearse, T., and Selkoe, D. J. (2023) Identification of the Aβ37/42 peptide ratio in CSF as an improved Aβ biomarker for Alzheimer's disease, *Alzheimers Dement19*, 79-96.

[25] Elangovan, M., Day, R. N., and Periasamy, A. (2002) Nanosecond fluorescence resonance energy transfer-fluorescence lifetime imaging microscopy to localize the protein interactions in a single living cell, *J Microsc 205*, 3-14.

[26] Liu, L., Lauro, B. M., Wolfe, M. S., and Selkoe, D. J. (2021) Hydrophilic loop 1 of Presenilin-1 and the APP GxxxG transmembrane motif regulate γ-secretase function in generating Alzheimer-causing Aβ peptides, *J Biol Chem. 296:100393*.

[27] Maesako, M., Houser, M. C. Q., Turchyna, Y., Wolfe, M. A.-O., and Berezovska, O. (2022) Presenilin/γ-Secretase Activity Is Located in Acidic Compartments of Live, *J Neurosci 42*, 145-154.

[28] McKendell, A. K., Houser, M. C. Q., Mitchell, S. P. C., Wolfe, M. S., Berezovska, O., and Maesako, M. (2022) In-Depth Characterization of Endo-Lysosomal Aβ in Intact Neurons, *Biosensors (Basel) 12*, 663.

[29] Herrup, K. (2015) The case for rejecting the amyloid cascade hypothesis, *Nat Neurosci 18*, 794-799.

[30] Storandt, M., Balota, D. A., Aschenbrenner, A. J., and Morris, J. C. (2014) Clinical and psychological characteristics of the initial cohort of the Dominantly Inherited Alzheimer Network (DIAN), *Neuropsychol 28*, 19-29.

[31] McKay, N. S., Gordon, B. A., Hornbeck, R. C., Dincer, A., Flores, S., Keefe, S. J., Joseph-Mathurin, N., Jack, C. R., Koeppe, R., Millar, P. R., Ances, B. M., Chen, C. D., Daniels, A., Hobbs, D. A., Jackson, K., Koudelis, D., Massoumzadeh, P., McCullough, A., Nickels, M. L., Rahmani, F., Swisher, L., Wang, Q., Allegri, R. F., Berman, S. B., Brickman, A. M., Brooks, W. S., Cash, D. M., Chhatwal, J. P., Day, G. S., Farlow, M. R., la Fougère, C., Fox, N. C., Fulham, M., Ghetti, B., Graff-Radford, N., Ikeuchi, T., Klunk, W., Lee, J. H., Levin, J., Martins, R., Masters, C. L., McConathy, J., Mori, H., Noble, J. M., Reischl, G., Rowe, C., Salloway, S., Sanchez-Valle, R., Schofield, P. R., Shimada, H., Shoji, M., Su, Y., Suzuki, K., Vöglein, J., Yakushev, I., Cruchaga, C., Hassenstab, J., Karch, C., McDade, E., Perrin, R. J., Xiong, C., Morris, J. C., Bateman, R. J., and Benzinger, T. L. S. (2023) Positron emission tomography and magnetic resonance imaging methods and datasets within the Dominantly Inherited Alzheimer Network (DIAN), *Nat Neurosci 26*, 1449-1460.

[32] Schultz, S. A., Liu, L., Schultz, A. P., Fitzpatrick, C. D., Levin, R., Bellier, J. P., Shirzadi, Z., Joseph-Mathurin, N., Chen, C. D., Benzinger, T. L. S., Day, G. S., Farlow, M. R., Gordon, B. A., Hassenstab, J. J., Jack, C. R., Jr., Jucker, M., Karch, C. M., Lee, J. H., Levin, J., Perrin, R. J., Schofield, P. R., Xiong, C., Johnson, K. A., McDade, E., Bateman, R. J., Sperling, R. A., Selkoe, D. J., and Chhatwal, J. P. (2024) γ-Secretase activity, clinical features, and biomarkers of autosomal dominant Alzheimer's disease: cross-sectional and longitudinal analysis of the Dominantly Inherited Alzheimer Network observational study (DIAN-OBS), *Lancet Neurol*, online ahead of print.

[33] Guo, X., Li, H., Yan, C., Lei, J., Zhou, R., and Shi, Y. (2024) Molecular mechanism of substrate recognition and cleavage by human γ-secretase, *Science 384*, 1091-1095.

[34] Odorčić, I., Hamed, M. B., Lismont, S., Chávez-Gutiérrez, L., and Efremov, R. G. (2024) Apo and Aβ46-bound γ-secretase structures provide insights into amyloid-β processing by the APH-1B isoform, *Nat Commun 15*, 4479.

[35] Zhou, R., Yang, G., Guo, X., Zhou, Q., Lei, J., and Shi, Y. (2019) Recognition of the amyloid precursor protein by human γ-secretase, *Science 363*, eaaw0930

[36] Sato, C., Takagi, S., Tomita, T., and Iwatsubo, T. (2008) The C-terminal PAL motif and transmembrane domain 9 of presenilin 1 are involved in the formation of the catalytic pore of γ-secretase, *J Neurosci 28*, 6264-6271.

[37] Wang, B., Yang, W., Wen, W., Sun, J., Su, B., Liu, B., Ma, D., Lv, D., Wen, Y., Qu, T., Chen, M., Sun, M., Shen, Y., and Zhang, X. (2010) γ-Secretase gene mutations in familial acne inversa, *Science 330*, 1065.

[38] Sun, L., Zhou, R., Yang, G., and Shi, Y. (2017) Analysis of 138 pathogenic mutations in presenilin-1 on the in vitro production of Aβ42 and Aβ40 peptides by γ-secretase, *Proc Natl Acad Sci USA 114*, E476-E485.

[39] Wolfe, M. S. (2024) Amyloid-independent pathogenesis for Alzheimer’s disease: implications for drug design, *Med Chem Res*, DOI: 10.1007/s00044-024-03261-9.

[40] Cummings, J., Zhou, Y., Lee, G., Zhong, K., Fonseca, J., and Cheng, F. (2023) Alzheimer's disease drug development pipeline: 2023, *Alzheimers Dement 9*, e12385.

[41] Li, Y. M., Lai, M. T., Xu, M., Huang, Q., DiMuzio-Mower, J., Sardana, M. K., Shi, X. P., Yin, K. C., Shafer, J. A., and Gardell, S. J. (2000) Presenilin 1 is linked with γ-secretase activity in the detergent solubilized state, *Proc Natl Acad Sci USA 97*, 6138-6143.

[42] Bolduc, D. M., Selkoe, D. J., and Wolfe, M. S. (2017) Enzymatic Assays for Studying Intramembrane Proteolysis, *Meth Enzymol 584*, 295-308.

[43] Fraering, P. C., Ye, W., Strub, J. M., Dolios, G., LaVoie, M. J., Ostaszewski, B. L., Van Dorsselaer, A., Wang, R., Selkoe, D. J., and Wolfe, M. S. (2004) Purification and Characterization of the Human γ-Secretase Complex, *Biochemistry 43*, 9774-9789.

[44] Osenkowski, P., Li, H., Ye, W., Li, D., Aeschbach, L., Fraering, P. C., Wolfe, M. S., Selkoe, D. J., and Li, H. (2009) Cryoelectron microscopy structure of purified γ-secretase at 12 Å resolution, *J Mol Biol 385*, 642-652.

SUPPLEMENTAL INFORMATION

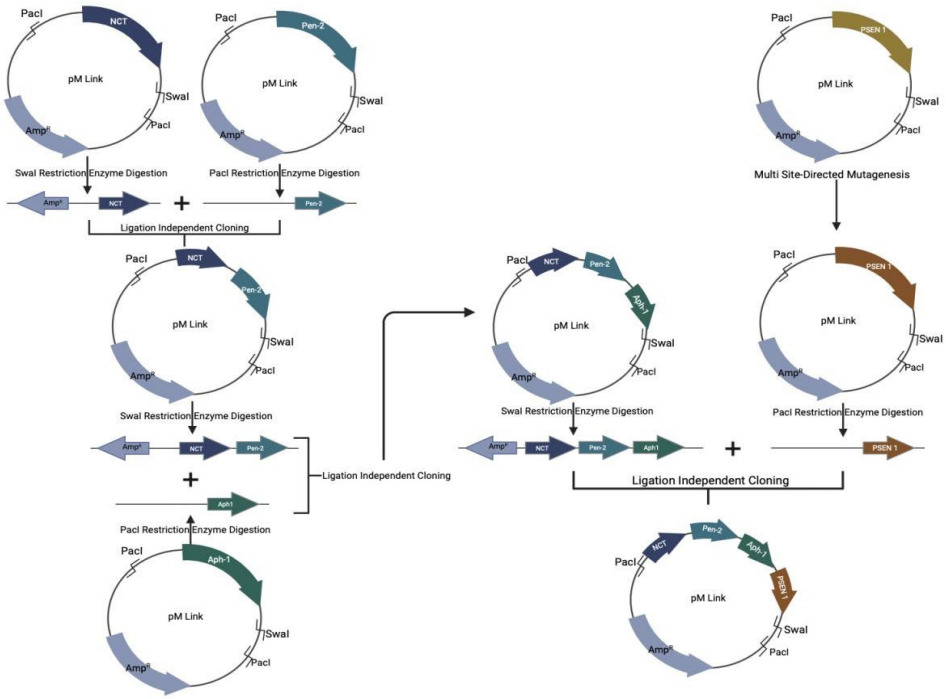

Figure S1. Process of installing PSEN-1 mutations into full γ-secretase plasmid. Step-by-step Ligation-Independent Cloning (LIC) was developed in *E. coli*, along with restriction digestion of both the insert and vector, enabling the successful insertion of mutations. A tricistronic plasmid containing genetic codes for three membrane protein components of the γ-secretase complex, including nicastrin, presenilin enhancer (Pen2), and anterior pharynx-defective 1 (Aph1) was prepared. This plasmid was created in two steps: initially, Nicastrin and Pen2 were combined using LIC in *E. coli* and restriction digestion, forming a bicistronic plasmid. Subsequently, the bicistronic plasmid was further modified by including Aph1 through another round of restriction digestion and LIC in *E. coli*, resulting in a tricistronic plasmid. Finally, Multi-Site Directed Mutagenesis was used to mutate PSEN1, and this monocistronic construct was incorporated into the tricistronic plasmid through additional rounds of restriction digestion and LIC in *E. coli*. Figure 1 illustrates the details of this process.

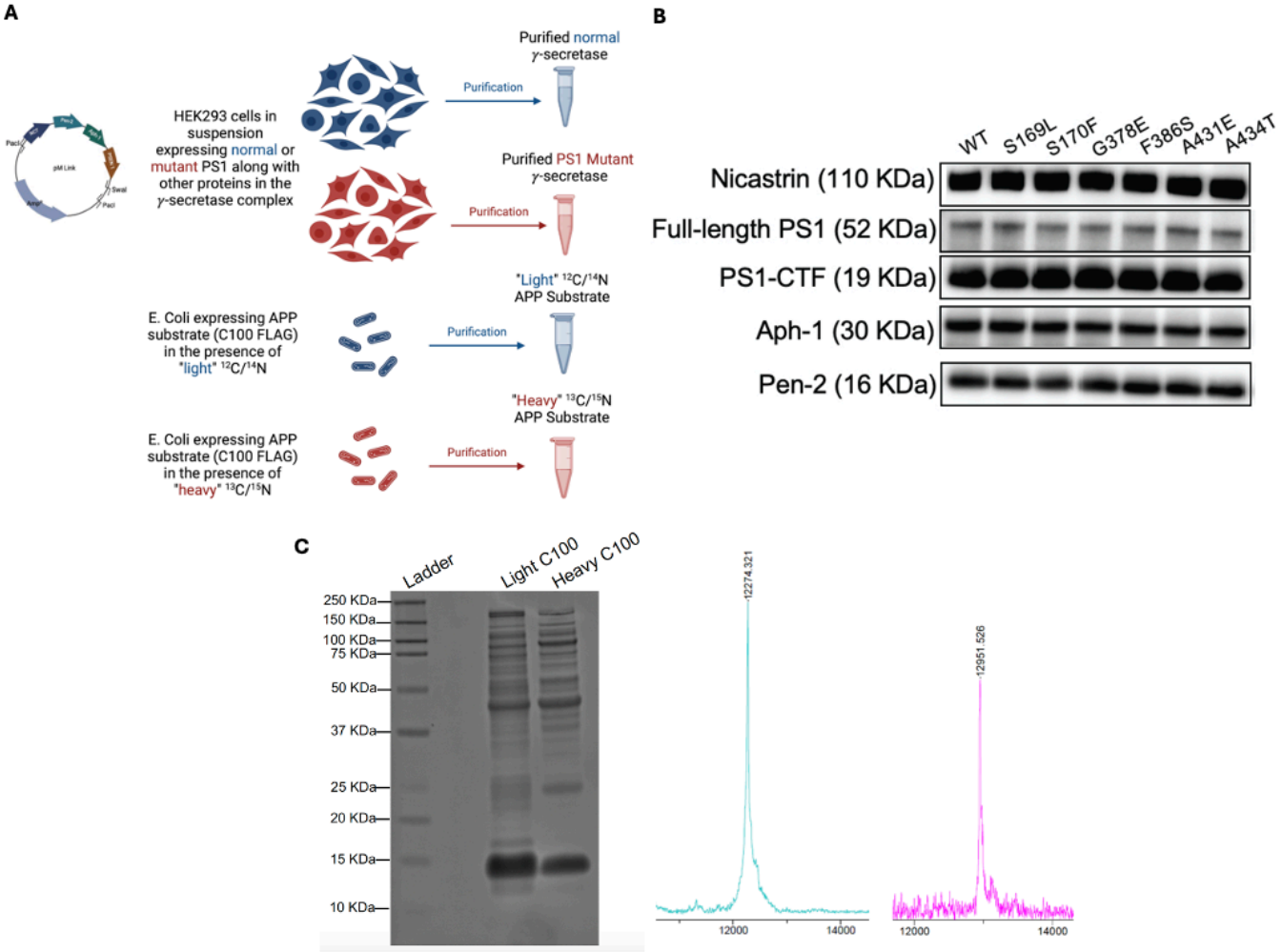

Figure S2. Expression, purification, and quality control of C100 substrate and γ-secretase. (A) Schematic of expression and purification of γ-secretase and C100. (B) Western blot analysis of all components within expressed and purified WT and FAD-mutant γ-secretase complexes, normalized to protein concentration using Pen2 intensity. (C) Characterization of light and heavy isotopic C100-FLAG substrates. The identity and purity of both C100-FLAG variants were assessed using SDS-PAGE with silver staining and MALDI-TOF mass spectrometry. The theoretical masses are 12272.89 for the light C100-FLAG and 12951.6 for the heavy C100-FLAG. Prior to reactions, concentrations were normalized based on band intensity in western blotting.

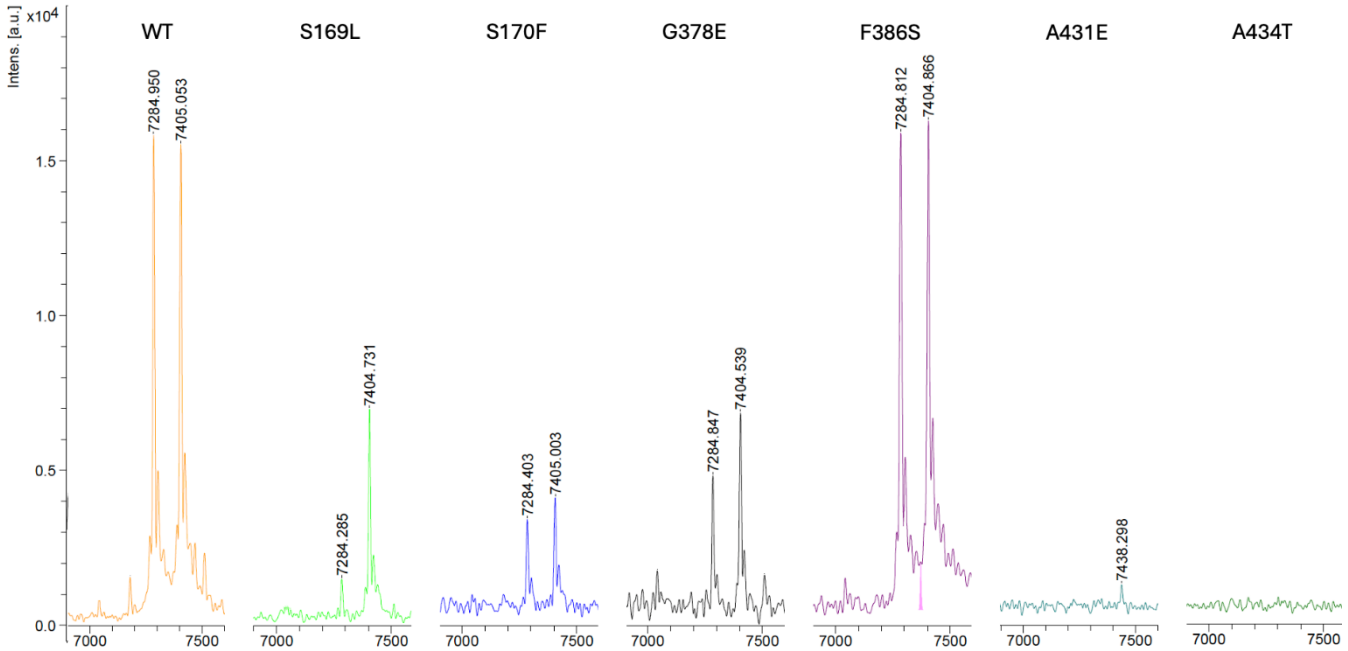

Figure S3. MALDI-TOF MS detection of AICD 50-99 and AICD 49-99 products from wild-type (WT) and six PSEN1 FAD-mutant γ-secretase. The theoretical mass for AICD 50-99 is 7286.02 Da, and for AICD 49-99 is 7406.12 Da.

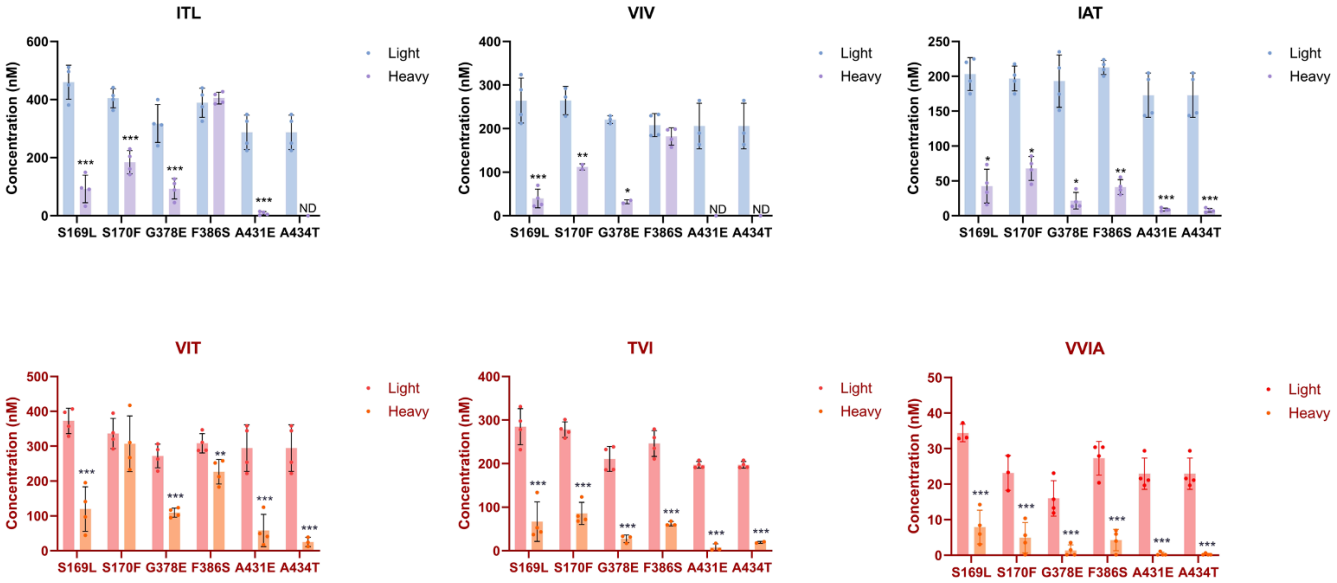

Figure S4. Alzheimer-mutant PSEN-1 affects the processive proteolysis of C99 by γ-secretase. Bar graphs illustrating coproduct formation at each trimming step. For the Aβ49/Aβ40 pathway, blue and purple bars represent the first, second, and third trimming steps. Red and orange bars denote trimming steps for the Aβ48/Aβ38 pathway. Blue/red and Purple/orange bars indicate coproducts formed by WT and FAD-mutant γ-secretase, respectively. For each graph, n = 4 and statistical significance was determined using unpaired two-tailed t-tests comparing FAD mutants with WT (*p < 0.05, **p < 0.01, ***p < 0.001). (Note: This figure is another representation of Figure 2C).

Table S1. Cross Reactivity of Aβ43 peptide with Aβ40 and Aβ42 ELISA kits.

A

Concentration of Aβ43 (pg/mL)	Cross reactivity (Read: pg/mL)
15.63	8.9
31.25	10.5
62.5	12.0
125	14.2
250	28.8
500	67.4
1000	203.3
2500	867.4
5000	OF
10000	OF
20000	OF
200000	OF
1000000	OF

B

Concentration of Aβ43 (pg/mL)	Cross reactivity (Read: pg/mL)
7.8	15.8
15.63	11.4
31.25	22.6
62.5	7.1
125	15.0
250	20.7
500	32.5
1000	41.6
50000	93.4
100000	104.2
200000	116.3
1000000	117.4

A. Cross-reactivity of Aβ43 with Aβ42 in ELISA assays. Various concentrations of Aβ43 (ranging from 15.63 pg/ml to 1000000 pg/ml) were tested using Aβ42-specific ELISA kits. The instrument readings for each concentration are displayed, indicating significant cross-reactivity starting at 250 pg/ml (0.06 nM) of Aβ43. (Note: “OF” stands for overflow)

B. Cross-reactivity of Aβ43 with Aβ40 in ELISA assays. Different concentrations of Aβ43 (ranging from 7.8 to 1,000,000 pg/ml) were assessed using ELISA kits specific for Aβ40. The resulting instrument readings for each concentration are presented, revealing cross-reactivity beginning at 500 pg/ml (0.12 nM) of Aβ43.